Acta Biomaterialia 39 (2016) 146–155

Contents lists available at ScienceDirect

Acta Biomaterialia

journal homepage: www.elsevier.com/locate/actabiomat

Full length article

Multi-biofunction of antimicrobial peptide-immobilized silk fibroin nanofiber membrane: Implications for wound healing

Dae Woong Song [a], Shin Hwan Kim [b], Hyung Hwan Kim [a], Ki Hoon Lee [a], Chang Seok Ki [a,**], Young Hwan Park [a,c,d,*]

[a] Department of Biosystems and Biomaterials Science and Engineering, Seoul National University, Seoul 08826, Republic of Korea
[b] Product Tech Transfer Team, Ajinomoto Genexine Corporation, Incheon 21991, Republic of Korea
[c] Center for Food and Bioconvergence, Seoul National University, Seoul 08826, Republic of Korea
[d] Research Institute of Agriculture and Life Sciences, Seoul National University, Seoul 08826, Republic of Korea

ARTICLE INFO

Article history:
Received 30 December 2015
Received in revised form 18 April 2016
Accepted 4 May 2016
Available online 6 May 2016

Keywords:
Antimicrobial peptide
Immobilization
Wound dressing
Silk fibroin
Nanofiber

ABSTRACT

An antimicrobial peptide motif (Cys-KR12) originating from human cathelicidin peptide (LL37) was immobilized onto electrospun SF nanofiber membranes using EDC/NHS and thiol-maleimide click chemistry to confer the various bioactivities of LL37 onto the membrane for wound care purposes. Surface characterizations revealed that the immobilization density of Cys-KR12 on SF nanofibers could be precisely controlled with a high reaction yield. The Cys-KR12-immobilized SF nanofiber membrane exhibited antimicrobial activity against four pathogenic bacterial strains (*Staphylococcus aureus*, *Staphylococcus epidermidis*, *Escherichia coli*, and *Pseudomonas aeruginosa*) without biofilm formation on the membrane surface. It also facilitated the proliferation of keratinocytes and fibroblasts and promoted the differentiation of keratinocytes with enhanced cell-cell attachment. In addition, immobilized Cys-KR12 significantly suppressed the LPS-induced TNF-α expression of monocytes (Raw264.7) cultured on the membrane. These results suggest that a Cys-KR12-immobilized SF nanofiber membrane, which has multiple biological activities, would be a promising candidate as a wound dressing material.

Statement of Significance

This research article reports various bioactivities of an antimicrobial peptide on electrospun silk fibroin nanofiber membrane. Recently, human cathelicidin peptide LL37 has been extensively explored as an alternative antibiotic material. It has not only a great antimicrobial activity but also a wide variety of bioactivities which can facilitate wound healing process. Especially, many studies on immobilization of LL37 or its analogues have shown the immobilization technique could improve performance of wound dressing materials or tissue culture matrices. Nevertheless, so far studies have only focused on the bactericidal effect of immobilized peptide on material surface. On the other hand, we tried to evaluate multi-biofunction of immobilized antimicrobial peptide Cys-KR12, which is the shortest peptide motif as an analogue of LL37. We fabricated silk fibroin nanofiber membrane as a model wound dressing by electrospinning and immobilized the antimicrobial peptide. As a result, we confirmed that the immobilized peptide can play multi-role in wound healing process, such as antimicrobial activity, facilitation of cell proliferation and keratinocyte differentiation, and inhibition of inflammatory cytokine expression. These findings have not been reported and can give an inspiration in wound-care application.

1. Introduction

Wound treatment is one of the most important and challenging healthcare issues. In the United States, 6.5 million patients suffer from chronic wounds and spend 25 billion US dollars annually on their treatment [1]. Without proper treatments, skin wounds are often exposed to bacterial infection, which prolongs inflammation,

* Corresponding author at: Department of Biosystems and Biomaterials Science and Engineering, Seoul National University, Seoul 08826, Republic of Korea (Y.H. Park).
** Co-corresponding author at: Department of Biosystems and Biomaterials Science and Engineering, Seoul National University, Seoul 08826, Republic of Korea (C.S. Ki).
E-mail addresses: ki.cs@snu.ac.kr (C.S. Ki), nfchempf@snu.ac.kr (Y.H. Park).

http://dx.doi.org/10.1016/j.actbio.2016.05.008
1742-7061/

disturbs re-epithelialization, inhibits collagen production, and delays wound healing [2]. In addition, once bacteria adhere to a solid surface, they form biofilms, which are sessile communities of bacteria that are embedded with extracellular polymeric substances. These biofilms protect bacteria from the immune system and antibiotics and release endotoxins that cause sepsis, which can lead to death [2,3]. Therefore, preventing bacterial infection and biofilm formation is of utmost importance in wound treatment.

In wound treatment, wound dressing is typically used to facilitate wound healing. A wide variety of biocompatible materials (e.g., silk, gelatin, cellulose, chitosan, alginate, polyurethane, poly (lactide-co-glycolide), polyvinyl alcohol, and poly-ε-caprolactone) can be used [4] in various forms (e.g., nanofiber, woven fabric, film, foam, hydrogel, hydrocolloid, and hydrofiber) for wound dressing fabrication [5]. Silk fibroin (SF), a primary constituent of silk proteins, is one of the most attractive biomaterials. It has excellent biocompatibility and low immunogenicity with good mechanical properties [6]. Furthermore, SF can be readily functionalized on its plentiful functional groups (e.g., carboxyl, amine, hydroxyl, and phenol groups) [7]. Thus, SF-based materials have been studied as promising biomaterials for use as tissue engineering scaffolds and surgical sutures [6]. SF has outstanding performance as a wound dressing material, and accordingly various types of fabrication techniques have been attempted [8]. Electrospinning is an attractive method for SF wound dressing fabrication because electrospun fiber has a large surface area with a high porosity [5,9]. However, the intact electrospun SF nanofiber is limited as a wound dressing material because it can paradoxically provide a preferred environment for infectious bacteria [10].

To prevent bacterial infection and biofilm formation on both skin wounds and dressing material, antibiotics such as penicillin and methicillin have been used. However, the use of traditional antibiotics has been reduced due to an emergence of antibiotic resistant bacteria [11]. Alternatively, other types of antimicrobial materials (e.g., quaternary ammonium compounds [12], silver ions or nanoparticles [13], or antimicrobial polymers [14]) have been tried for wound care. In particular, silver-containing materials present excellent antimicrobial effects [15]. However, these alternative materials have either considerable adverse effect (e.g., cytotoxicity, environmental issues) or low efficacy [12,13,16–18].

In recent years, antimicrobial peptides (AMPs) have received great interest as alternative antimicrobial materials. Generally, AMPs, which exist in mammals, insects, fishes, amphibians, and even some bacteria, play a crucial role in protecting the host from invasive bacteria, fungi, or viruses in conjunction with other immune responses [19,20]. Although AMPs have diverse structures, they share common structural characteristics such as cationic and amphiphilic domains with α-helical conformation. It is believed that such a structure plays a key role in antimicrobial activity by disrupting the bacterial cell membrane [19,20]. AMPs exhibit not only the rapid onset of bacterial killing but also a broad-spectrum of antimicrobial activity with a high efficacy. Furthermore, they do not cause bacterial resistance and therefore are relatively safe in long-term use [21]. For example, the antimicrobial peptide nisin was approved by the Food and Drug Administration (FDA) as a food preservative [22]. In addition, many pharmaceutical companies have been trying to develop AMPs for therapeutic use, and some have been applied in clinical trials [23].

KR12 (KRIVKRIKKWLR) is the shortest antimicrobial motif (residue 18–29) of the human cathelicidin peptide (LL37) [24–26], which is secreted from various human immunocytes and epithelial cells [27]. In addition to antimicrobial activity, LL37 exhibits various bioactivities such as the neutralization of lipopolysaccharides (LPS) [28], the modulation of the inflammatory response [29], and the promotion of re-epithelialization (i.e., migration, proliferation, and the differentiation of epithelial cells) [30–34], which result in an acceleration of the wound healing process [35,36]. In spite of this multi-functionality, the use of LL37 or KR12 is limited because of potential cytotoxicity and susceptibility to proteolysis [37–40]. To reduce its cytotoxicity and increase its antimicrobial stability, AMPs are often immobilized onto surfaces of materials in various biomedical applications such as urinary catheters [41–43], bone or dental implants [44–46], and artificial corneas [47]. Nevertheless, only a few studies have attempted to use AMPs as wound dressing application [48–50], and no study has tested the multi-function of biomaterial-surface-immobilized KR12 peptide.

In this study, we immobilized an antimicrobial peptide (Cys-KR12) onto an electrospun SF nanofiber membranes via a thiol-maleimide coupling method and investigated its antimicrobial activity against different types of pathogenic bacteria with varying immobilization densities. Additionally, the various bioactivities (i.e., proliferation, differentiation, and pro-inflammatory cytokine expression) of the Cys-KR12-immobilized SF nanofiber membrane were evaluated with respect to wound healing.

2. Materials and methods

2.1. Materials

To obtain SF, *Bombyx mori* cocoons were boiled in 0.3% (w/v) sodium oleate and 0.2% (w/v) sodium carbonate solution at 100 °C for 1 h. Degummed cocoons were washed in deionized water and dried. SF solution was obtained by dissolving the degummed cocoons in 9.3 M LiBr (Kanto Chemical) solution at 60 °C for 4 h. The SF solution was then dialyzed against deionized water using cellulose acetate membrane (MWCO: 12–14 kDa) for 3 days, which was followed by freeze-drying. Cys-KR12 (CKRIVKRIKKWLR, analogue-3 of original KR12 from [25], >95% purity) (Fig. S1) was purchased from BeadTech Inc. and all other unspecified chemicals were purchased from Sigma-Aldrich.

2.2. Fabrication of the Cys-KR12-immbolized SF nanofiber membrane

For electrospinning, SF solution was prepared by dissolving regenerated SF sponge in formic acid at 11% (w/v). Then, the dope solution was transferred to a syringe and electrospun onto parchment paper at 13 kV and 0.3 mL/h for 24 h in ambient conditions. After electrospinning, the SF nanofiber membrane was insolubilized by soaking in ethanol for 1 h. Peptide immobilization was conducted by a three-step process with a combination of EDC/NHS chemistry and thiol-maleimide click chemistry (Fig. 1). Briefly, the carboxylic acid groups of SF were activated by N-(3-dimethylaminopropyl)-N′-ethylcarbodiimide hydrochloride (EDC) (0.4 mg/mL) and N-hydroxysuccinimide (NHS) (0.6 mg/mL) in 2-(N-morpholino)ethanesulfonic acid (MES) buffer (pH 6.0) for 15 min at room temperature. The carboxyl-activated SF nanofiber membrane was transferred into phosphate buffered saline (PBS) (pH 7.4) and then reacted with N-(2-aminoethyl)maleimide (AEM) linker (0.2 mg/mL) for 2 h at room temperature before washing three times with deionized water. The AEM-conjugated SF nanofiber membrane (SF-AEM) was reacted with various concentrations of Cys-KR12 solution (50, 100, 200, and 500 μg/mL) in PBS for 4 h at room temperature and subsequently washed three times with deionized water. Sample IDs are designated as the concentration of Cys-KR12 solution used in the immobilization (Table 1).

2.3. Surface characterizations

The surface morphology of the SF nanofiber membrane was observed using field-emission scanning electronic microscopy

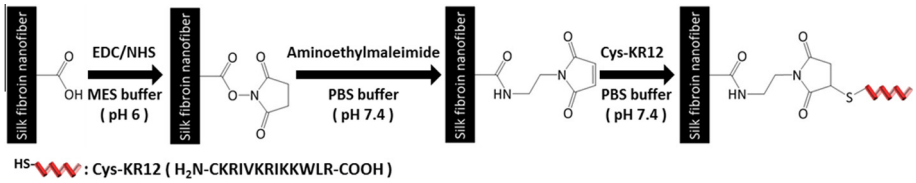

Fig. 1. Schematic of immobilization of Cys-KR12 peptide onto the SF nanofiber membrane surface using EDC/NHS and thiol-maleimide click chemistry.

Table 1
Sample IDs and Cys-KR12 concentrations used for peptide immobilization on SF nanofiber membranes.

Sample ID	Pristine SF	K50	K100	K200	K500
Concentration of Cys-KR12 (μg/mL)	–	50	100	200	500

(FE-SEM) (SUPRA, Carl Zeiss). Mean fiber diameter and the distribution of fiber diameter were determined by counting 100 points from obtained images using Image-J software. The amount of immobilized Cys-KR12 was quantified by Ellman's assay based on absorbance change of the solution by the reaction between thiol group of Cys-KR12 and Ellman's reagent (5,5′-dithiobis-(2-nitroben zoic acid), DTNB). 20 μL aliquots of un-reacted/reacted solutions were transferred into 96-well plate, and 200 μL of Ellman's reagent (Thermo Scientific) solution was added into each well. After 15 min incubation at room temperature, optical density at 412 nm was measured using a microplate reader (Synergy HT, Bio-Tek instruments). Immobilization density and reaction yield were calculated by the following equations.

$$\text{Immobilized peptide} = (\text{Initial Conc.} - \text{Final Conc.}) \times (\text{Volume of solution}) \quad (1)$$

$$\text{Immobilization density} = (\text{Immobilized peptide})/(\text{Surface area}) \quad (2)$$

$$\text{Reaction yield } (\%) = (\text{Initial Conc.} - \text{Final Conc.})/(\text{Initial Conc.}) \times 100 \quad (3)$$

Surface zeta potentials of Pristine SF, SF-AEM, and K200 were measured using an electrophoretic light scattering spectrophotometer (ELS) (ELS-8000, Otsuka Electronics) in deionized water (pH 7.0) at 25 °C. The surface elemental compositions of Pristine SF and K200 were measured using an X-ray photoelectron spectrometer (XPS) (SIGMA PROBE, Thermo Scientific) equipped with a monochromatic Al K_α X-ray source ($h\nu$ = 1486.6 eV). Survey scan spectra were scanned from 0.0 to 1000.0 eV in 1.0 eV steps, and high resolution XPS spectra were scanned from 278.0 to 298.0 eV for C1s and from 392.0 to 412.0 eV for N1s in 0.1 steps. Chemical shifts of high-resolution spectra were analyzed on C1s hydrocarbon at 285.0 eV.

2.4. Antimicrobial test

Two Gram-positive bacteria (*Staphylococcus aureus* (ATCC 25923) and *Staphylococcus epidermidis* (ATCC 12228)) and two Gram-negative bacteria (*Escherichia coli* (ATCC 9637) and *Pseudomonas aeruginosa* (ATCC 15692)) were grown on Luria-Bertani (LB) (BD Difco) agar plates, and a single colony of each strain was isolated and subsequently cultured in LB broth at 37 °C overnight. The bacterial suspension was adjusted to a desired concentration by measuring the optical density at 600 nm using a microplate reader. Minimum inhibitory concentrations (MICs) of Cys-KR12 were tested against *S. aureus*, *S. epidermidis*, *E. coli*, and *P. aeruginosa* by a broth microdilution method. Cys-KR12 was dissolved in PBS at various concentrations (1–40 μg/mL). Then, 50 μL of bacterial suspension (1×10^6 CFU/mL) and 50 μL of peptide solutions were added into a 96-well polypropylene plate and incubated at 37 °C for 20 h with shaking. Optical density at 600 nm was measured every hour using a microplate reader to monitor bacterial growth. MIC was defined as the minimum peptide concentration that inhibited bacterial growth. The surface antimicrobial activity of the Cys-KR12-immobilized SF nanofiber membrane was tested against *S. aureus*, *S. epidermidis*, *E. coli*, and *P. aeruginosa* by a modified JIS Z 2801 method. Pristine SF was used as control for comparison with Cys-KR12-immobilized SF nanofiber membranes. Briefly, 50 μL of bacterial suspension (1×10^5 CFU/mL) was inoculated onto samples and incubated at 37 °C for 4 h. After incubation, samples were transferred into 24-well plate with 1 mL of PBS and then sonicated for 5 min in an ultrasound bath (KODO JAC-4020, 40 kHz) to re-suspend adhered bacteria. 10-fold serial dilutions of sonicated solution were prepared, and 50 μL of the diluted solution was inoculated onto LB agar plates. Then, plates were incubated at 37 °C for 24 h, and the number of colonies was counted. For long-term surface antimicrobial stability test, K200 samples were soaked in PBS at 37 °C and 4 °C for 3 weeks. At each time point, an antimicrobial activity test was performed against *S. aureus* and *E. coli* with the previously described method. Bacterial reduction was calculated by measuring the CFU of Pristine SF (M_1) and K200 (M_2) with the following equation.

$$\text{Bacterial reduction } (\%) = (M_1 - M_2)/M_1 \times 100 \quad (4)$$

The biofilm formation of *S. aureus* and *E. coli* on Pristine SF and K200 was observed using FE-SEM. For this, 50 μL of the bacterial suspension (1×10^6 CFU/mL) was inoculated onto samples (Pristine SF and K200) and incubated at 37 °C for 24 h. After incubation, samples were washed with PBS three times and fixed with 2.5% (v/v) glutaraldehyde solution for 24 h, which was followed by dehydration in serially diluted ethanol solutions.

2.5. Cell culture

Human keratinocytes (HaCaT), human dermal fibroblasts (NHDF), and murine monocytes (Raw264.7) were cultured in Dulbecco's Modified Eagle's Medium (DMEM) (Corning) supplemented with 10% (v/v) fetal bovine serum (FBS) and 1% (v/v) penicillin/streptomycin at 37 °C and 5% CO_2. The cytotoxicity of Cys-KR12 was evaluated by the methylthiazolyldiphenyl-tetrazolium bromide (MTT) assay. HaCaT and NHDF cells were seeded on 96-well plates at 10,000 cells/well and incubated for 24 h. Then, the culture media were replaced with Cys-KR12 dissolved in serum-free DMEM (0–1000 μg/mL). After 24 h, 10 μL of MTT solution (5 mg/mL) was added into culture medium and incubated at 37 °C for 4 h. The optical density at 570 nm was measured using a microplate reader, and relative cell viability was calculated relative to non-treated control. The LD50 was determined by DoseResp sigmoidal curve fitting using Origin software. The proliferation of HaCaT and NHDF cells was examined by measuring metabolic activity and total DNA content. Nanofiber membranes (Pristine SF, K200, and K500) were

placed in 96-well plates, and the harvested cells were seeded at 2000 cells/well. Metabolic activity was measured with the CellTiter-Blue® cell viability assay according to the manufacturer's instructions. Briefly, 20 μL of 10 × CellTiter-Blue® reagent (Promega) diluted in DMEM was added into each well at each time point. After 5 h incubation, 150 μL of culture medium was transferred into black 96-well plates, and fluorescence intensity was measured using a microplate reader (ex/em, 540/560 nm). Total DNA content was also measured by QuantiFluor® dsDNA assay according to the manufacturer's instructions. Briefly, after 1- and 10-day incubations, samples were washed with PBS three times and transferred into 1.5 mL microtubes. DNA was extracted and purified with the TIANamp Genomic DNA kit (Qiagen) according to the manufacturer's instructions. Then, 100 μL of the purified DNA samples and 100 μL of QuantiFlour® dsDNA reagent (Promega) diluted in TE buffer were transferred into black 96-well plates. After a 5-min incubation at room temperature, fluorescence intensity was measured (ex/em, 504/531 nm). Metabolic activity and total DNA content were normalized by the intensity on day 1.

2.6. Western blotting

Samples (Pristine SF, K200, and K500) were placed in 48-well plates, and cells were seeded at 20,000 cells/well. After a 10-day culture, attached cells were washed with PBS three times, and cytoplasmic proteins were extracted using cell lysis RIPA buffer (Amresco). Protein concentrations were measured with the BCA assay kit (Thermo Scientific). Then, the proteins were subjected to SDS-PAGE, and separated proteins were transferred onto PVDF membranes (Bio-Rad) using Trans-Blot® Turbo™ Transfer System (Bio-Rad), followed by blocking with 5% (w/v) non-fat milk (Bio-Rad) in PBST (0.05% Tween 20). Primary antibodies and secondary antibody used in western blots were mouse anti-human beta actin loading control antibody (BA3R), mouse anti-human involucrin antibody (SY5), and HRP-conjugated goat anti-mouse IgG (H + L) secondary antibody (Thermo Scientific). The blots were incubated for 1 h with the appropriate primary antibodies and secondary antibody, which were diluted with SignalBoost™ Immunoreaction Enhancer Kit (Merck Millipore). The membrane was developed with West Pico Chemiluminescent Substrate (Thermo Scientific), and band images were obtained using ChemiDoc™ XRS + System with Image Lab™ Software (Bio-Rad).

2.7. Immunofluorescence

After the 10-day culture, samples were washed with PBS three times and fixed with 4% (w/v) paraformaldehyde solution for 10 min. The fixed cells were permeabilized with 0.25% (v/v) Triton X-100 in PBS and blocked with 1% (w/v) BSA in PBST overnight. Permeabilized cells were sequentially treated with mouse anti-human involucrin antibody (SY5) and Alexa Fluor® 488-conjugated goat anti-mouse IgG (H + L) secondary antibody (Thermo Scientific) for 1 h. Then, cells were stained with rhodamine-phalloidin (Molecular Probes) and DAPI (Molecular Probes) for the visualization of F-actin and nuclei. The stained cells were observed with a confocal laser scanning microscope (CLSM) (TCS SP8, Leica).

2.8. Enzyme-linked immunosorbent assay

Samples (Pristine SF, K200, and K500) were placed in 96-well plates, and Raw264.7 cells were seeded at 50,000 cells/well. The seeded cells were incubated overnight (12 h) and stimulated with LPS (10 ng/mL) for 6 h. Tissue culture plate (TCP) and Cys-KR12 (20 μg/mL) were used as negative and positive controls, respectively. Before and after LPS stimulation, cell culture media were collected, and the TNF-α concentration was measured by ELISA kit (Novex) according to the manufacturer's instructions.

2.9. Statistics

All experiments were performed in triplicate, and data are presented as the means ± SD. One-way ANOVA with Bonferroni post hoc test was performed to determine the statistical significance between Pristine SF and indicated groups ($^{*}p < 0.05$, $^{**}p < 0.01$, $^{***}p < 0.001$).

3. Results

3.1. Immobilization of Cys-KR12 onto the SF nanofiber membrane

We obtained the SF nanofiber membrane without bead formation via electrospinning. The average diameter of as-spun fibers was approximately 350 nm, and the immobilization process did not change fiber morphology or size distribution (Fig. S2). As shown in Fig. 2A, the reaction yield was greater than 90% at all Cys-KR12 concentrations. The immobilization density of Cys-KR12 was linearly proportional to the Cys-KR12 concentration in the reaction medium in the range of 0.15–1.43 nmol per square centimeter. After immobilization, the change in surface zeta potential was measured. K200 group showed positive values, whereas both Pristine SF and SF-AEM showed negative values (Fig. 2B). As shown in Fig. 3, although the change in the composition of atoms (C, N, and O) was negligible, the peak compositions of C1s peaks significantly changed after surface immobilization (Table 2). In

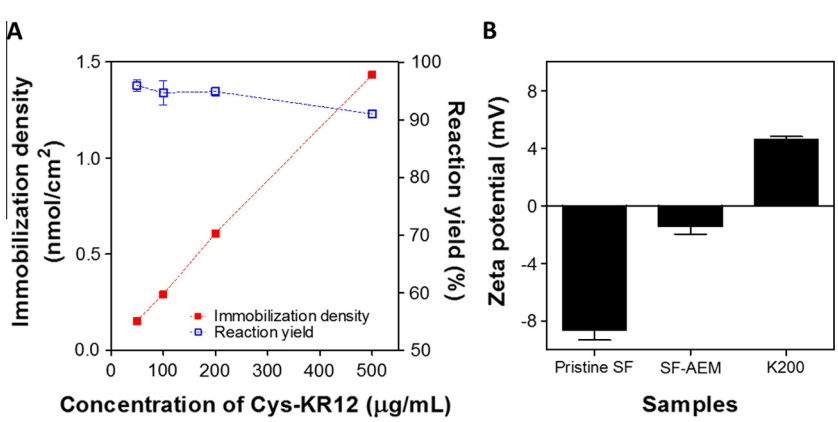

Fig. 2. (A) Immobilized peptide densities on SF nanofiber surface and reaction yields at varying Cys-KR12 concentrations in reaction media; (B) surface zeta potentials of Pristine SF, SF-AEM, and K200 at pH 7.0 (n = 3, mean ± SD).

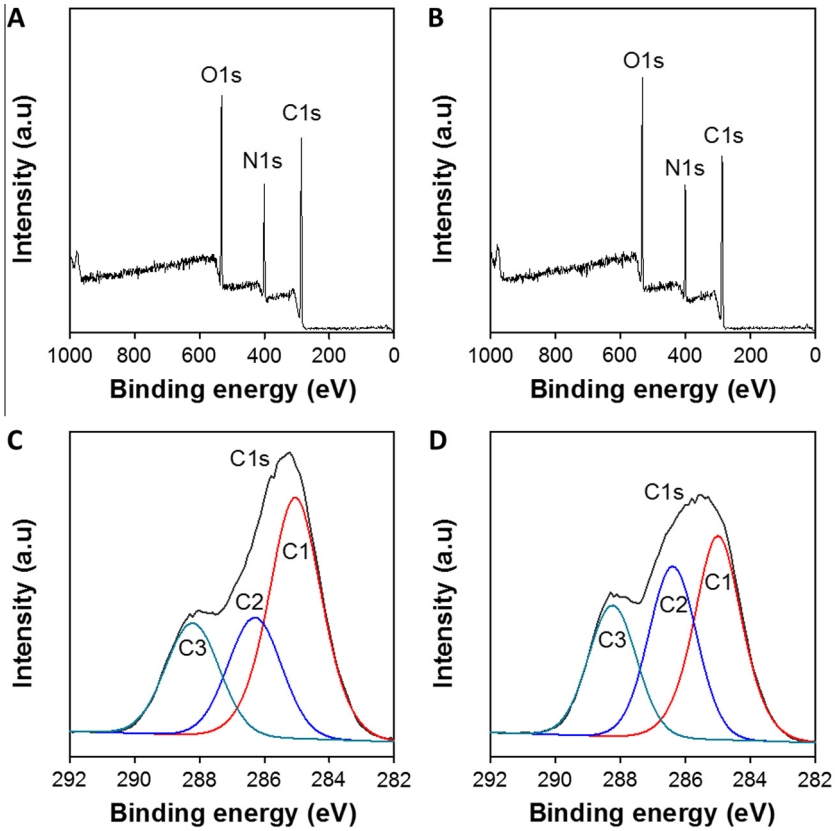

Fig. 3. XPS analysis results for characterization of surface elemental composition. Survey scan spectra of (A) Pristine SF and (B) K200; high resolution C1 s spectra of (C) Pristine SF and (D) K200.

Table 2
Surface elemental compositions of Pristine SF and K200 obtained by XPS analysis.

Sample	C1 (at%) (C—C, C—H)	C2 (at%) (C—N, C—O)	C3 (at%) (O=C—N)	C (at %)	N (at %)	N/C ratio
Pristine SF	51.26	25.14	23.60	81.79	18.21	0.22
K200	40.75	33.61	25.64	80.63	19.37	0.24

Fig. 3C and D, both peak C2 at 286.5 eV for C—N or C—O carbon and peak C3 at 288.5 eV for the anti-screened carbon of the peptide backbone (O=C—N) increased relatively, whereas peak C1 at 285 eV for aliphatic carbon (C—C or C—H) decreased after immobilization.

3.2. Antimicrobial activity of the Cys-KR12-immobilized SF nanofiber membrane

The antimicrobial activity of surface-immobilized Cys-KR12 against four bacterial strains is presented in Fig. 4A. All of the Cys-KR12-immobilized SF nanofiber membranes significantly suppressed bacterial growth compared with Pristine SF. The inhibition effect increased as immobilization density increased, resulting in no bacterial survival on K200 and K500 regardless of bacterial strain. Fig. 4B and C show that the antimicrobial activity of K200 against *S. aureus* and *E. coli* was maintained for a long-term storage condition. At 4 °C, K200 retained 99% bacterial reduction for both strains after a 3-week storage. However, the bacterial reduction of K200 against *S. aureus* decreased with time over a week in PBS at 37 °C, whereas K200 exhibited a stable inhibitory effect on *E. coli*. The antimicrobial activity of K200 was also confirmed by observing biofilm formation on the membrane. As shown in Fig. 5, no biofilm was formed on K200 for *S. aureus* or *E. coli*, but a large number of bacteria attached and agglomerated on Pristine SF to create biofilms.

3.3. Facilitated proliferation of HaCaT and NHDF cells on the Cys-KR12-immobilized SF nanofiber membrane

Prior to performing cell proliferation assays on the Cys-KR12-immobilized SF nanofiber membrane, the cytotoxicity of Cys-KR12 was examined. Cys-KR12 was not cytotoxic to HaCaT or NHDF cells in the range of 1–100 μg/mL, but cell viability decreased above 100 μg/mL (Fig. S4). Fig. 6 presents changes of metabolic activity and the DNA content of HaCaT and NHDF cells grown on K200 and K500, which have shown strong bactericidal activity. We observed that both the metabolic activity and the DNA content of HaCaT cells increased with an increase of the immobilization density of Cys-KR12. K500 especially showed a significant increase in DNA content compared with Pristine SF (Fig. 6B). For NHDF cells, the metabolic activity and DNA content also tended to increase in the presence of immobilized Cys-KR12, similar to the result of HaCaT cells (Fig. 6C and D).

3.4. Differentiation of HaCaT cells on the Cys-KR12-immobilized SF nanofiber membrane

The differentiation of HaCaT cells cultured on SF nanofiber membranes was evaluated by measuring involucrin expression. As shown in Fig. 7A, the expression of involucrin increased in the presence of immobilized Cys-KR12. K500 showed the highest band intensity, which was approximately 2 and 3 times higher than

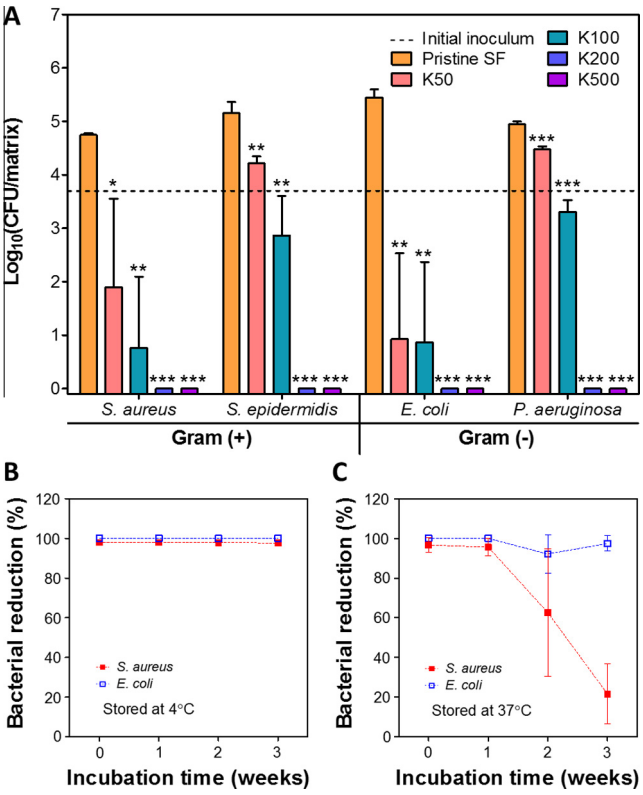

Fig. 4. (A) Log(CFU/matrix) of Pristine SF and Cys-KR12 immobilized SF nanofiber membrane measured by modified JIS Z 2801 method (n = 3, mean ± SD); long-term bactericidal activity at (B) 4 °C and (C) 37 °C storage. Bacterial reduction (%) was calculated based on CFU of Pristine SF (n = 3, mean ± SD).

Pristine SF and TCP, respectively (Fig. 7B). The higher expression of involucrin was also observed by immunofluorescence (Fig. 7C). The involucrin signal (green) was much more intense in K200 and K500 compared with either TCP or Pristine SF. Interestingly, cells were more densely packed in the presence of Cys-KR12 (i.e., K200 and K500), indicating increased cell-cell attachment.

3.5. Inhibition of TNF-α expression in Raw264.7 cells cultured on the Cys-KR12-immobilized SF nanofiber membrane

To evaluate the immunomodulatory effects of immobilized Cys-KR12, Raw264.7 cells were cultured on the Cys-KR12-immobilized SF nanofiber membrane and stimulated with LPS. As shown in Fig. 8, there was no significant difference in TNF-α concentration between sample groups except for the soluble Cys-KR12 treated group. After LPS stimulation, the concentrations of TNF-α dramatically increased in TCP and Pristine SF groups. In contrast, the increase of TNF-α concentration was relatively lower and TNF-α expression was more suppressed at a higher Cys-KR12 immobilization density (i.e., K500).

4. Discussion

AMPs have been highlighted recently for their various roles (e.g., promoting re-epithelialization and angiogenesis, neutralizing LPS, and acting as immunomodulators) in the wound healing process [19,28–30,32,34–36]. To incorporate AMP into wound dressing materials, various techniques such as immobilization and sustained release have been attempted. The immobilization technique is preferred because it can not only reduce the cytotoxicity of AMP but also increase the stability of AMP in a physiological environment [51,52]. The immobilization of AMP on wound dressing material is a very effective method to prolong the antimicrobial activity of wound dressing with a limited amount of AMPs. Nevertheless, most studies on AMP immobilization have only focused on the antimicrobial effect of immobilized AMPs for various biomedical applications. Thus, it is worthy to evaluate the various functions of immobilized AMP in the wound healing process.

We chose KR12 as a model antimicrobial peptide. KR12 is the shortest antimicrobial motif of LL37; its antimicrobial and antiendotoxic activity is well known, and synthesis is relatively simple. To increase coupling efficiency while minimizing the activity loss of KR12 in the immobilization process, we utilized click-chemistry by adding cysteine to the N-terminus of KR12. This peptide design is very important because the antimicrobial activity of AMPs largely depends on peptide orientation on the surface [53,54]. For the wound dressing material, the SF nanofiber membrane was chosen. A large specific surface area of electrospun

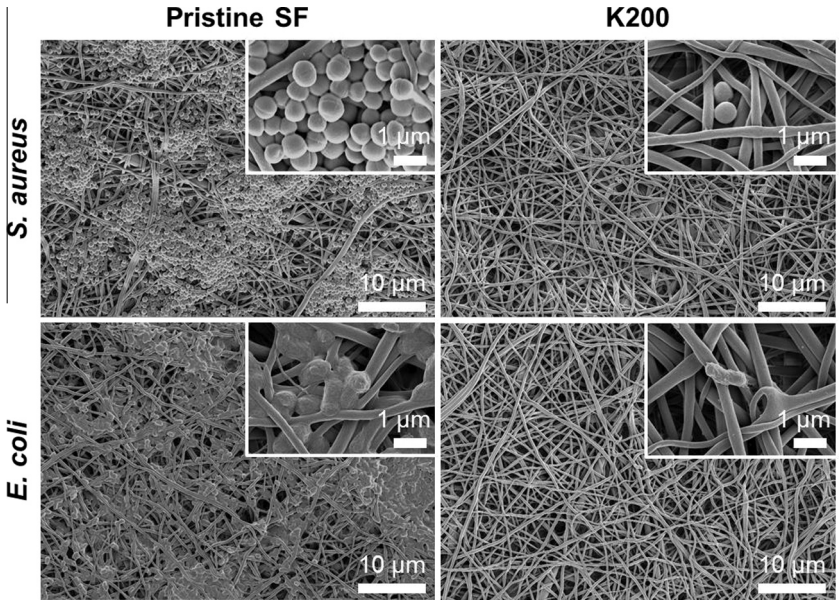

Fig. 5. FE-SEM images of 24 h-cultured *S. aureus* and *E. coli* on Pristine SF (left column) and K200 (right column).

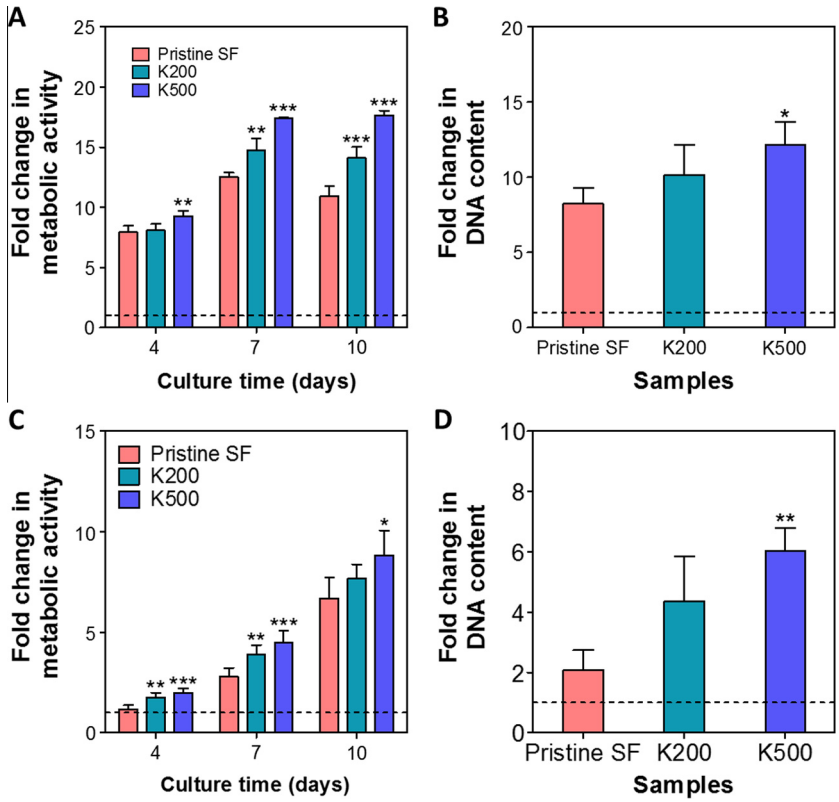

Fig. 6. (A) Metabolic activity and (B) DNA content of HaCaT cells cultured on SF nanofiber membranes (Pristine SF, K200, and K500) for 10-day culture. (C) Metabolic activity and (D) DNA content of NHDF cells cultured on SF nanofiber membranes (Pristine SF, K200, and K500) for 10-day culture. Dot lines indicate each value of Pristine SF on day 1 as 1-fold (n = 3, mean ± SD).

nanofiber membrane provides an appropriate platform for the immobilization of AMP. The immobilization of Cys-KR12 was conducted with a maleimide linker (AEM) by Michael addition, which forms covalent linkage between thiol and maleimide groups for site specific immobilization [42,53]. This method allowed the precise control of the immobilization density of Cys-KR12; this density was linearly proportional to the concentration of Cys-KR12 in the reaction solution (Fig. 2A). After the immobilization, both the positive surface charge and the binding energy shift at the C1 s peak (Figs. 2B and 3) confirm that lysine- and arginine-rich peptide were bound on the SF nanofiber membrane.

Before evaluating the antimicrobial activity of immobilized Cys-KR12, we measured the MIC of soluble Cys-KR12 against four different bacterial strains. Cys-KR12 inhibited the growth of all of the strains in the range of 4–8 μg/mL (Fig. S3). This low MIC value was comparable to the previously reported MIC of KR12 [25]. As expected, the immobilized Cys-KR12 also exhibited antimicrobial activity. Even the K100 group showed a decreased viability for all of the bacterial strains. At a higher immobilization density of Cys-KR12 (i.e., K200 or K500), the peptide-immobilized SF nanofiber membrane exhibited a high bactericidal activity, completely preventing biofilm formation as shown in Fig. 5. In general, the antimicrobial activity of surface-immobilized AMP is significantly reduced compared with soluble AMP [55]. Therefore, in many cases, AMPs have been immobilized with a flexible spacer (e.g., poly(ethylene glycol)), which can retain the activity of AMP [53,55]. Alternatively, the decreased antimicrobial activity can be compensated by simply increasing the immobilization density of AMP although direct coupling and short cross-linker are utilized for AMP immobilization [51]. Of course, it is very difficult to compare the effectiveness of immobilized AMP to that of soluble AMP because the surface density and the concentration in solution are not directly comparable. Nevertheless, K200 and K500 groups revealed antimicrobial effects against four different bacterial strains similar to soluble Cys-KR12. It might be because Cys-KR12 was properly oriented from the surface. Hilpert et al. [54] demonstrated that the hydrophobic residue of AMP plays a key role in insertion of AMP into bacterial cell membrane. Therefore, hydrophobic residue of AMP should be located farthest from the immobilization site. In this study, we immobilized Cys-KR12 through its N-terminal cysteine because it has its hydrophobic residue at its C-terminus.

Another important factor in evaluating the antimicrobial property of wound dressing materials is the longevity of the bactericidal activity either in preservation or on the wound site. For long-term surface antimicrobial activity test, K200 was used since its Cys-KR12 immobilization density was the lowest condition for exhibiting sufficient bactericidal activity against all the bacterial strains. As shown in Fig. 4B and C, the Cys-KR12-immobilized SF nanofiber membrane (K200) did not lose its initial bactericidal activity after 3 weeks at 4 °C. This result means that 4 °C is the proper storage temperature for maintaining antimicrobial activity of the Cys-KR12-immobilized SF nanofiber membrane. On the other hand, the antimicrobial activity retained only within 1 week at 37 °C storage. This reduction of antimicrobial activity might be due to an inactivation of peptide by thermal denaturation. Especially, alpha-helical structure of LL37-like peptides plays an important role in the bactericidal action. Such a structure of peptide or protein easily changes by temperature, resulting in loss of its innate functions [56,57]. Nevertheless, such a result implies that the membrane would continuously exhibit antimicrobial activity at a wound site without requiring frequent dressing changes or treatment with antibiotics.

In wound healing process, cell proliferation is very important factor especially for re-epithelialization [2]. The immobilized Cys-

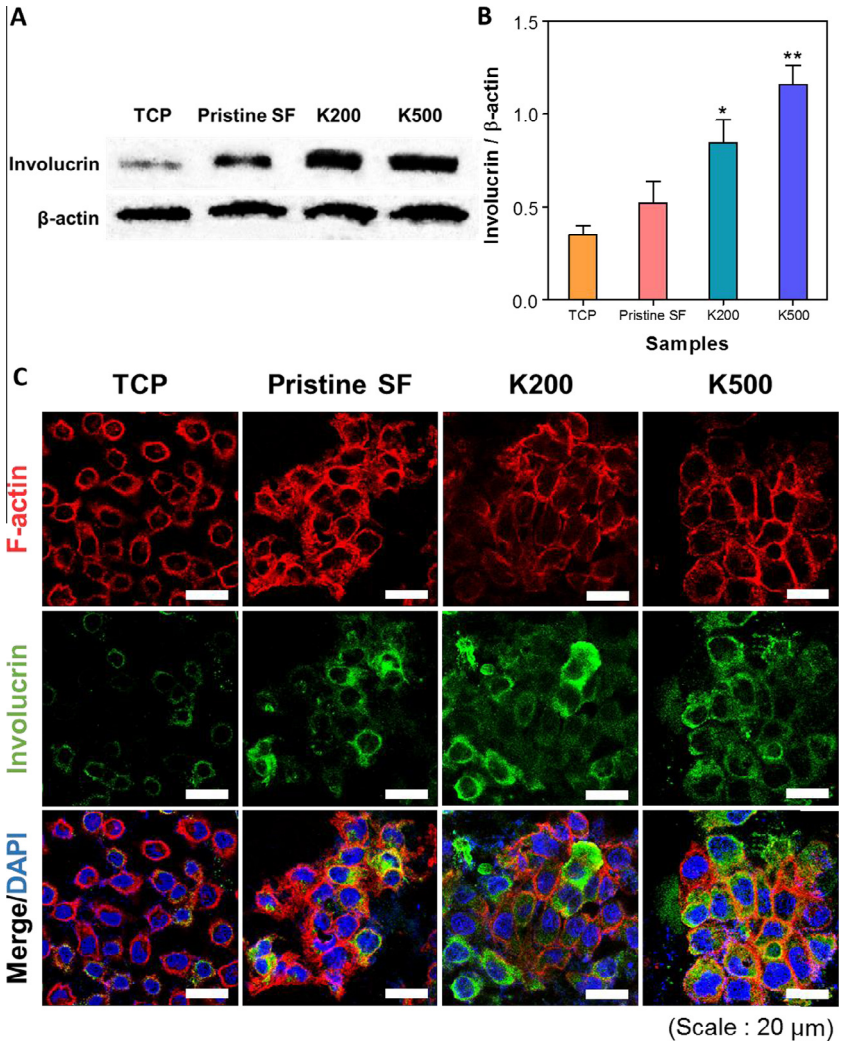

Fig. 7. (A) Representative western blot band images of involucrin as a keratinocyte differentiation marker. (B) Relative expression levels of involucrin obtained from band intensity analysis (n = 3, mean ± SD). Asterisks indicate significant difference compared with Pristine SF. (C) Confocal immunofluorescence images of human keratinocytes (HaCaT) cultured on TCP, pristine SF, K200, and K500 (red, F-actin; green, involucrin; blue, DAPI).

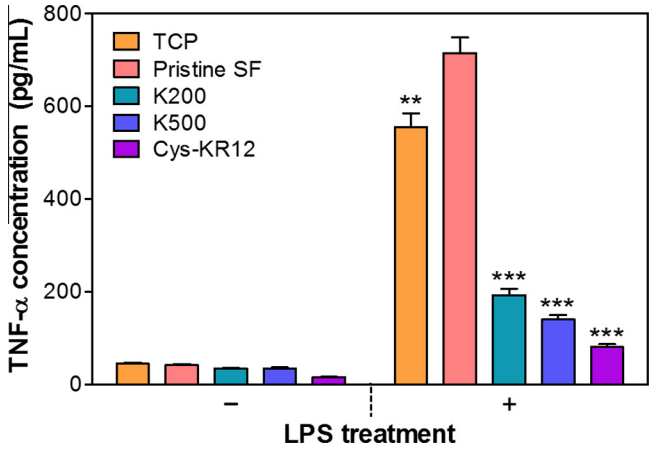

Fig. 8. Secreted TNF-α from Raw264.7 cells stimulated by LPS (10 ng/mL) for 6 h. Cells were cultured on TCP, Pristine SF, K200, and K500 before LPS stimulation. TCP and Cys-KR12 peptide (20 μg/mL) were used as negative and positive control for each (n = 3, mean ± SD). Asterisks indicate significant difference compared with Pristine SF.

KR12 facilitated the proliferation of HaCaT and NHDF cells on the SF nanofiber membrane without cytotoxicity. Although soluble Cys-KR12 showed cytotoxicity on HaCaT and NHDF cells at a high concentration (>100 μg/mL) (Fig. S4), it was much higher than MIC values (4–8 μg/mL). It might be due to different susceptibilities of mammalian and bacterial cells for cytotoxic effect, indicating the immobilized Cys-KR12 of an optimal concentration can elicit positive effects on wound healing process minimizing its cytotoxicity. Interestingly, we also found that the immobilized Cys-KR12 promoted the involucrin expression of HaCaT cells (Fig. 7). Involucrin expressed at the granular layer of epidermis is a representative marker protein when keratinocytes reach the final stage of differentiation. It is also a very important indicator for re-epithelialization in would healing process. Therefore, such an increase of involucrin expression indicates that more keratinocytes were differentiated into granular form. In other words, it implies that final stage of wound healing can be facilitated by Cys-KR12-immobilized silk nanofiber membrane. These effects of KR12 on cell proliferation and differentiation have not been reported, and the mechanism is also unclear. However, we speculate that the effects of immobilized KR12 peptides on differentiation of keratinocytes and on proliferation of keratinocytes and fibroblasts are similar to those previously reported for LL37, which activates

MAPK/ERK signaling pathway via the transactivation of EGFR, which leads to cell migration, proliferation, and differentiation [30,58–60]. These results suggest that surface-immobilized Cys-KR12 peptide can promote the re-epithelialization of skin epithelial cells, which is crucial for rapid wound healing.

Another important function of immobilized Cys-KR12 was the suppression of LPS-induced TNF-α expression in monocytes (i.e., Raw264.7 cells). Overexpressed TNF-α not only causes chronic inflammation but also upregulates the expression of various matrix metalloproteinases (MMPs) although TNF-α also plays an important role in inflammation response and wound healing. These effects by a flood of TNF-α at wound sites often prolong the wound healing process [2]. Thus, the control of TNF-α expression in a proper range is crucial for rapid wound healing. It is well known that human cathelicidin peptide suppresses LPS-induced TNF-α expression and that it can prevent septic shock or sepsis by binding LPS, LPS binding protein (LBP), or CD14 receptor [28,29]. The KR12 analogue used in this study was thought to directly bind LBP or CD14 receptor [25]. As expected, the LPS-induced TNF-α expression of Raw264.7 cells was significantly repressed on the Cys-KR12-immobilized SF nanofiber membrane compared with the TCP and non-immobilized SF nanofiber membrane groups (Fig. 8). This inhibition might be due to the direct binding of Cys-KR12 on LBP or the CD14 receptor, which indicates that immobilized Cys-KR12 peptide retained the unique properties of KR12. Taken together, the various bioactivities of the Cys-KR12-immobilized SF nanofiber membrane provide this material with a great advantage as a wound dressing material.

5. Conclusion

In summary, we have shown that the antimicrobial peptide Cys-KR12 can be immobilized onto a SF nanofiber membrane at a desired density with a high reaction yield and that the Cys-KR12-immobilized SF nanofiber membrane exhibited antimicrobial activity against different bacterial strains. Its bactericidal activity was fully maintained in PBS at 4 °C for 3 weeks. In addition, the Cys-KR12-immobilized SF nanofiber membrane showed various activities on keratinocytes, fibroblasts, and monocytes, which play important roles in the wound healing process. It promoted not only the proliferation and differentiation of HaCaT cells but also the proliferation of NHDF cells. For Raw264.7 cells stimulated by LPS, the Cys-KR12-immobilized SF nanofiber membrane significantly inhibited TNF-α expression to a similar extent as a soluble KR12 peptide. Therefore, these results indicate that the Cys-KR12-immobilized SF nanofiber membrane has great feasibility as a wound dressing material.

Acknowledgement

This work was supported by the National Research Foundation of Korea (NRF) funded by the Ministry of Science, ICT and Future Planning (NRF-2015R1A2A2A03002680).

Appendix A. Supplementary data

Supplementary data associated with this article can be found, in the online version, at http://dx.doi.org/10.1016/j.actbio.2016.05.008.

References

[1] C.K. Sen, G.M. Gordillo, S. Roy, R. Kirsner, L. Lambert, T.K. Hunt, F. Gottrup, G.C. Gurtner, M.T. Longaker, Human skin wounds: a major and snowballing threat to public health and the economy, Wound Repair Regen. 17 (2009) 763–771.
[2] R. Edwards, K.G. Harding, Bacteria and wound healing, Curr. Opin. Infect. Dis. 17 (2004) 91–96.
[3] F. Siedenbiedel, J.C. Tiller, Antimicrobial polymers in solution and on surfaces: overview and functional principles, Polymers 4 (2012) 46–71.
[4] G.D. Mogosanu, A.M. Grumezescu, Natural and synthetic polymers for wounds and burns dressing, Int. J. Pharm. 463 (2014) 127–136.
[5] M. Abrigo, S.L. McArthur, P. Kingshott, Electrospun nanofibers as dressings for chronic wound care: advances, challenges, and future prospects, Macromol. Biosci. 14 (2014) 772–792.
[6] C. Vepari, D.L. Kaplan, Silk as a biomaterial, Prog. Polym. Sci. 32 (2007) 991–1007.
[7] A.R. Murphy, D.L. Kaplan, Biomedical applications of chemically-modified silk fibroin, J. Mater. Chem. 19 (2009) 6443–6450.
[8] E.S. Gil, B. Panilaitis, E. Bellas, D.L. Kaplan, Functionalized silk biomaterials for wound healing, Adv. Healthc. Mater. 2 (2013) 206–217.
[9] Z.G. Wang, L.S. Wan, Z.M. Liu, X.J. Huang, Z.K. Xu, Enzyme immobilization on electrospun polymer nanofibers: an overview, J. Mol. Catal. B-Enzym. 56 (2009) 189–195.
[10] J. Kaur, R. Rajkhowa, T. Afrin, T. Tsuzuki, X. Wang, Facts and myths of antibacterial properties of silk, Biopolymers 101 (2014) 237–245.
[11] H. Nikaido, Multidrug resistance in bacteria, Annu. Rev. Biochem. 78 (2009) 119–146.
[12] T. Thorsteinsson, M. Masson, K.G. Kristinsson, M.A. Hjalmarsdottir, H. Hilmarsson, T. Loftsson, Soft antimicrobial agents: synthesis and activity of labile environmentally friendly long chain quaternary ammonium compounds, J. Med. Chem. 46 (2003) 4173–4181.
[13] B.S. Atiyeh, M. Costagliola, S.N. Hayek, S.A. Dibo, Effect of silver on burn wound infection control and healing: review of the literature, Burns 33 (2007) 139–148.
[14] M. Kong, X.G. Chen, K. Xing, H.J. Park, Antimicrobial properties of chitosan and mode of action: a state of the art review, Int. J. Food Microbiol. 144 (2010) 51–63.
[15] E.K. Mooney, C. Lippitt, J. Friedman, Silver dressings, Plast. Reconstr. Surg. 117 (2006) 666–669.
[16] J.W. Loh, G. Yeoh, M. Saunders, L.Y. Lim, Uptake and cytotoxicity of chitosan nanoparticles in human liver cells, Toxicol. Appl. Pharmacol. 249 (2010) 148–157.
[17] V.K. Poon, A. Burd, In vitro cytotoxicity of silver: implication for clinical wound care, Burns 30 (2004) 140–147.
[18] M.V. Park, A.M. Neigh, J.P. Vermeulen, L.J. de la Fonteyne, H.W. Verharen, J.J. Briede, H. van Loveren, W.H. de Jong, The effect of particle size on the cytotoxicity, inflammation, developmental toxicity and genotoxicity of silver nanoparticles, Biomaterials 32 (2011) 9810–9817.
[19] R.E. Hancock, H.G. Sahl, Antimicrobial and host-defense peptides as new anti-infective therapeutic strategies, Nat. Biotechnol. 24 (2006) 1551–1557.
[20] M. Zasloff, Antimicrobial peptides of multicellular organisms, Nature 415 (2002) 389–395.
[21] A. Parisien, B. Allain, J. Zhang, R. Mandeville, C.Q. Lan, Novel alternatives to antibiotics: bacteriophages, bacterial cell wall hydrolases, and antimicrobial peptides, J. Appl. Microbiol. 104 (2008) 1–13.
[22] J. Cleveland, T.J. Montville, I.F. Nes, M.L. Chikindas, Bacteriocins: safe, natural antimicrobials for food preservation, Int. J. Food Microbiol. 71 (2001) 1–20.
[23] J.L. Fox, Antimicrobial peptides stage a comeback, Nat. Biotechnol. 31 (2013) 379–382.
[24] G. Wang, Structures of human host defense cathelicidin LL-37 and its smallest antimicrobial peptide KR-12 in lipid micelles, J. Biol. Chem. 283 (2008) 32637–32643.
[25] B. Jacob, I.S. Park, J.K. Bang, S.Y. Shin, Short KR-12 analogs designed from human cathelicidin LL-37 possessing both antimicrobial and antiendotoxic activities without mammalian cell toxicity, J. Pept. Sci. 19 (2013) 700–707.
[26] B. Mishra, R.F. Epand, R.M. Epand, G. Wang, Structural location determines functional roles of the basic amino acids of KR-12, the smallest antimicrobial peptide from human cathelicidin LL-37, RSC Adv. 3 (2013) 19560–19571.
[27] D. Vandamme, B. Landuyt, W. Luyten, L. Schoofs, A comprehensive summary of LL-37, the factotum human cathelicidin peptide, Cell. Immunol. 280 (2012) 22–35.
[28] Y. Rosenfeld, N. Papo, Y. Shai, Endotoxin (lipopolysaccharide) neutralization by innate immunity host-defense peptides. Peptide properties and plausible modes of action, J. Biol. Chem. 281 (2006) 1636–1643.
[29] N. Mookherjee, K.L. Brown, D.M. Bowdish, S. Doria, R. Falsafi, K. Hokamp, F.M. Roche, R. Mu, G.H. Doho, J. Pistolic, J.P. Powers, J. Bryan, F.S. Brinkman, R.E. Hancock, Modulation of the TLR-mediated inflammatory response by the endogenous human host defense peptide LL-37, J. Immunol. 176 (2006) 2455–2464.
[30] G.S. Tjabringa, J. Aarbiou, D.K. Ninaber, J.W. Drijfhout, O.E. Sorensen, N. Borregaard, K.F. Rabe, P.S. Hiemstra, The antimicrobial peptide LL-37 activates innate immunity at the airway epithelial surface by transactivation of the epidermal growth factor receptor, J. Immunol. 171 (2003) 6690–6696.
[31] J.D. Heilborn, M.F. Nilsson, G. Kratz, G. Weber, O. Sorensen, N. Borregaard, M. Stahle-Backdahl, The cathelicidin anti-microbial peptide LL-37 is involved in re-epithelialization of human skin wounds and is lacking in chronic ulcer epithelium, J. Invest. Dermatol. 120 (2003) 379–389.
[32] S. Tokumaru, K. Sayama, Y. Shirakata, H. Komatsuzawa, K. Ouhara, Y. Hanakawa, Y. Yahata, X. Dai, M. Tohyama, H. Nagai, L. Yang, S. Higashiyama, A. Yoshimura, M. Sugai, K. Hashimoto, Induction of keratinocyte migration via transactivation of the epidermal growth factor receptor by the antimicrobial peptide LL-37, J. Immunol. 175 (2005) 4662–4668.

[33] R. Shaykhiev, C. Beisswenger, K. Kandler, J. Senske, A. Puchner, T. Damm, J. Behr, R. Bals, Human endogenous antibiotic LL-37 stimulates airway epithelial cell proliferation and wound closure, Am. J. Physiol. Lung Cell. Mol. Physiol. 289 (2005) L842–L848.
[34] T. Akiyama, F. Niyonsaba, C. Kiatsurayanon, T.T. Nguyen, H. Ushio, T. Fujimura, T. Ueno, K. Okumura, H. Ogawa, S. Ikeda, The human cathelicidin LL-37 host defense peptide upregulates tight junction-related proteins and increases human epidermal keratinocyte barrier function, J. Innate Immun. 6 (2014) 739–753.
[35] M. Carretero, M.J. Escamez, M. Garcia, B. Duarte, A. Holguin, L. Retamosa, J.L. Jorcano, M.D. Rio, F. Larcher, In vitro and in vivo wound healing-promoting activities of human cathelicidin LL-37, J. Invest. Dermatol. 128 (2008) 223–236.
[36] R. Ramos, J.P. Silva, A.C. Rodrigues, R. Costa, L. Guardao, F. Schmitt, R. Soares, M. Vilanova, L. Domingues, M. Gama, Wound healing activity of the human antimicrobial peptide LL37, Peptides 32 (2011) 1469–1476.
[37] S. Maher, S. McClean, Investigation of the cytotoxicity of eukaryotic and prokaryotic antimicrobial peptides in intestinal epithelial cells in vitro, Biochem. Pharmacol. 71 (2006) 1289–1298.
[38] F.F. Han, Y.F. Liu, Y.G. Xie, Y.H. Gao, C. Luan, Y.Z. Wang, Antimicrobial peptides derived from different animals: comparative studies of antimicrobial properties, cytotoxicity and mechanism of action, World J. Microbiol. Biotechnol. 27 (2011) 1847–1857.
[39] M. Bacalum, M. Radu, Cationic antimicrobial peptides cytotoxicity on mammalian cells: an analysis using therapeutic index integrative concept, Int. J. Pept. Res. Ther. 21 (2015) 47–55.
[40] A. Gronberg, L. Zettergren, M.S. Agren, Stability of the cathelicidin peptide LL-37 in a non-healing wound environment, Acta Derm. Venereol. 91 (2011) 511–515.
[41] X. Li, P. Li, R. Saravanan, A. Basu, B. Mishra, S.H. Lim, X. Su, P.A. Tambyah, S.S. Leong, Antimicrobial functionalization of silicone surfaces with engineered short peptides having broad spectrum antimicrobial and salt-resistant properties, Acta Biomater. 10 (2014) 258–266.
[42] B. Mishra, A. Basu, R.R.Y. Chua, R. Saravanan, P.A. Tambyah, B. Ho, M.W. Chang, S.S.J. Leong, Site specific immobilization of a potent antimicrobial peptide onto silicone catheters: evaluation against urinary tract infection pathogens, J. Mater. Chem. B 2 (2014) 1706–1716.
[43] K. Lim, R.R. Chua, H. Bow, P.A. Tambyah, K. Hadinoto, S.S. Leong, Development of a catheter functionalized by a polydopamine peptide coating with antimicrobial and antibiofilm properties, Acta Biomater. 15 (2015) 127–138.
[44] G. Gao, D. Lange, K. Hilpert, J. Kindrachuk, Y. Zou, J.T. Cheng, M. Kazemzadeh-Narbat, K. Yu, R. Wang, S.K. Straus, D.E. Brooks, B.H. Chew, R.E. Hancock, J.N. Kizhakkedathu, The biocompatibility and biofilm resistance of implant coatings based on hydrophilic polymer brushes conjugated with antimicrobial peptides, Biomaterials 32 (2011) 3899–3909.
[45] K.V. Holmberg, M. Abdolhosseini, Y. Li, X. Chen, S.U. Gorr, C. Aparicio, Bio-inspired stable antimicrobial peptide coatings for dental applications, Acta Biomater. 9 (2013) 8224–8231.
[46] W. Lin, C. Junjian, C. Chengzhi, S. Lin, L. Sa, R. Li, W. Yingjun, Multi-biofunctionalization of a titanium surface with a mixture of peptides to achieve excellent antimicrobial activity and biocompatibility, J. Mater. Chem. B 3 (2015) 30–33.
[47] X.W. Tan, T.W. Goh, P. Saraswathi, C.L. Nyein, M. Setiawan, A. Riau, R. Lakshminarayanan, S. Liu, D. Tan, R.W. Beuerman, J.S. Mehta, Effectiveness of antimicrobial peptide immobilization for preventing perioperative cornea implant-associated bacterial infection, Antimicrob. Agents Chemother. 58 (2014) 5229–5238.
[48] M. Pedrosa, C. Mouro, F. Nogueira, J. Vaz, I. Gouveia, Comparison of the antibacterial activity of modified-cotton with magainin I and LL-37 with potential as wound-dressings, in: J. Appl. Polym. Sci. 131 (2014).
[49] A.P. Gomes, J.F. Mano, J.A. Queiroz, I.C. Gouveia, Incorporation of antimicrobial peptides on functionalized cotton gauzes for medical applications, Carbohydr. Polym. 127 (2015) 451–461.
[50] T.D. Heunis, C. Smith, L.M. Dicks, Evaluation of a nisin-eluting nanofiber scaffold to treat *Staphylococcus aureus*-induced skin infections in mice, Antimicrob. Agents Chemother. 57 (2013) 3928–3935.
[51] K. Rapsch, F.F. Bier, M. Tadros, M. von Nickisch-Rosenegk, Identification of antimicrobial peptides and immobilization strategy suitable for a covalent surface coating with biocompatible properties, Bioconjug. Chem. 25 (2014) 308–319.
[52] L.Q. Bai, L.J. Zhu, S.J. Min, L. Liu, Y.R. Cai, J.M. Yao, Surface modification and properties of *Bombyx mori* silk fibroin films by antimicrobial peptide, Appl. Surf. Sci. 254 (2008) 2988–2995.
[53] M. Gabriel, K. Nazmi, E.C. Veerman, A.V. Nieuw Amerongen, A. Zentner, Preparation of LL-37-grafted titanium surfaces with bactericidal activity, Bioconjug. Chem. 17 (2006) 548–550.
[54] K. Hilpert, M. Elliott, H. Jenssen, J. Kindrachuk, C.D. Fjell, J. Korner, D.F. Winkler, L.L. Weaver, P. Henklein, A.S. Ulrich, S.H. Chiang, S.W. Farmer, N. Pante, R. Volkmer, R.E. Hancock, Screening and characterization of surface-tethered cationic peptides for antimicrobial activity, Chem. Biol. 16 (2009) 58–69.
[55] M. Bagheri, M. Beyermann, M. Dathe, Immobilization reduces the activity of surface-bound cationic antimicrobial peptides with no influence upon the activity spectrum, Antimicrob. Agents Chemother. 53 (2009) 1132–1141.
[56] L. Dong, J.J. Yang, Y. Wang, H. Liu, L.X. Mu, D.H. Lin, R. Lai, Structure-function relationship of antimicrobial peptide cathelicidin Pc-CATH1, Nat. Prod. Bioprospect. 2 (2012) 81–86.
[57] A. Tossi, L. Sandri, A. Giangaspero, Amphipathic, α-helical antimicrobial peptides, Biopolymers 55 (2000) 4–30.
[58] W. Zhang, H.T. Liu, MAPK signal pathways in the regulation of cell proliferation in mammalian cells, Cell Res. 12 (2002) 9–18.
[59] T. Efimova, A.M. Broome, R.L. Eckert, A regulatory role for p38 delta MAPK in keratinocyte differentiation. Evidence for p38 delta-ERK1/2 complex formation, in: J. Biol. Chem. 278 (2003) 34277–34285.
[60] G.D. Sharma, J. He, H.E. Bazan, P38 and ERK1/2 coordinate cellular migration and proliferation in epithelial wound healing: evidence of cross-talk activation between MAP kinase cascades, J. Biol. Chem. 278 (2003) 21989–21997.